Sui *et al. BMC Chemistry* (2026) 20:51
https://doi.org/10.1186/s13065-026-01743-y

BMC Chemistry

RESEARCH Open Access

Synthesis, structural characterization, DFT calculation, and antitumor activity of a new Co(II) complex based on 2-((2′-Carboxybenzyl) oxy)benzoic acid and 2,2′-bipyridine ligands

Bing-Lin Sui[1], Li-Hua Wang[2], Xi-Shi Tai[1*], Saud I. Al-Resayes[3], Mohammad Azam[3*] and An-Lin Wang[4*]

Abstract

In this work, a new Co(II) complex, abbreviated as $[Co(L)(bipy)(H_2O)_2]_n$ (**1**) was prepared using cobalt(II) acetate tetrahydrate, 2-((2′-carboxybenzyl)oxy)benzoic acid (H_2L), and 2,2′-bipyridine (bipy) ligands in a mixture solution of ethanol and water (v: v = 3: 1). The structure of the complex (**1**) was analyzed by elemental analysis (EA), infrared (IR) spectroscopy, ultraviolet-visible (UV-Vis) spectroscopy, thermogravimetric analysis (TG), and single-crystal X-ray diffraction techniques. The complex (**1**) crystallizes in the monoclinic space group *C*2/*c*, featuring a distorted octahedral $[CoO_4N_2]$ coordination sphere, by two oxygen atoms from the carboxylate groups of two 2-((2′-carboxybenzyl)oxy)benzoate (L) ligands, two oxygen atoms from coordinated water molecules, and two nitrogen atoms (N1 and N2) from a single 2,2′-bipyridine (bipy) ligand. Bridging carboxylate ligands (L) form a 1D chain, which extends into a 2D layer via π–π interactions of the 2,2′-bipyridine ligands (bipy). The DFT calculations of the complex (**1**) indicates that the HOMO is predominantly distributed on the oxygen and nitrogen atoms bonded to Co(II) ion, but the LUMO is mainly localized around distributed in the six-membered carbon ring adjacent to the Co(II) ion. Electrostatic potential calculation of the complex (1) shows that the regions with higher electrostatic potential are mainly located on the aromatic ring, whilst the lower electrostatic potential regions are primarily located near the oxygen and nitrogen atoms. The electrochemical behavior of the complex (**1**) was investigated in acetonitrile and 1 mol·L^{-1} sulfuric acid. In ACN/TBATFB, the complex (**1**) exhibits a well-defined, predominantly reversible Co(III)/Co(II) redox couple, indicating good electrochemical stability, whereas in 1 mol·L^{-1} H_2SO_4, a significantly different redox response with enhanced anodic currents and a prominent oxidation peak is observed, arising from the synergistic effect of ligand protonation–oxidation processes and the metal-centered

*Correspondence:
Xi-Shi Tai
taixs@wfu.edu.cn
Mohammad Azam
azam_res@yahoo.com
An-Lin Wang
jordan0309@126.com

Full list of author information is available at the end of the article

Co(III)/Co(II) redox couple under acidic conditions. The cytotoxicity of the complex (**1**) and $CoCl_2$ was evaluated against L02, PANC-1, and MCF7 cell lines using the MTT assay. The complex (**1**) exhibited lower IC_{50} values and higher selectivity for cancer cells than $CoCl_2$, attributable to improved cellular uptake and ROS-mediated oxidative stress, whereas free Co^{2+}, which stimulated cell proliferation at low concentrations, the complex (**1**) showed no growth-inducing effect, highlighting its potential as a cobalt-based anticancer agent.

Keywords 2-((2′-Carboxybenzyl)oxy)benzoic acid, 2,2′-bipyridine, Co(II) complex, Spectral characterization, Antitumor activity

Introduction

Transition metal coordination compounds have long intrigued the scientific community due to their structural diversity and wide-ranging applications in catalysis, materials science, and biomedicine [1–3]. Among these, cobalt(II) complexes are particularly significant due to their variable coordination geometries, redox behavior, and magnetic properties [4], making them ideal candidates for catalytic processes [5], molecular magnetism [6], photochemical systems [7], and biological applications [8, 9]. However, strategic selection of appropriate ligands is essential for tailoring these properties, as they influence the electronic environment, stability, and function of the complexes. Carboxylic acids, acting as monodentate or bridging multidentate ligands, form robust coordination networks, enabling the development of porous and stable materials for gas adsorption, separation, and various functional applications [10]. Carboxylates stabilize diverse coordination geometries and maintain metal-center electron density, thereby enabling the construction of MOFs [11], the development of efficient heterogeneous catalysts [12, 13], and the enhancement of biological activities [8, 9]. The inherent Lewis acidity of Co(II), along with the biocompatibility and structural flexibility of carboxylate ligands, enables strong interactions with biomolecules such as proteins and demonstrates antimicrobial activity against drug-resistant pathogens through ROS generation [14].

Over the years, cancer has remained a major global health challenge, with breast cancer being a leading cause of death among women, caused by the uncontrolled proliferation of malignant cells, and the ACS documented nearly 20 million new cases in 2024 [15]. Although cisplatin revolutionized chemotherapy [16], its severe toxicity and resistance issues [17] have prompted the search for safer and more effective alternatives. In recent years, transition-metal complexes have emerged as promising candidates owing to their diverse coordination capabilities, tunable redox and photochemical properties, and strong, selective interactions with biomolecular targets [18]. Notably, lighter metals such as Cu, Ni, Co, and Fe exhibit lower toxicity and better biocompatibility than platinum drugs [19], with essential metals such as copper and cobalt further enhancing therapeutic potential [20]. Among transition-metal complexes, cobalt complexes have gained prominence due to their structural versatility, accessible Co(II)/Co(III) redox chemistry, low toxicity, and inherent biological relevance [21]. As an essential trace element, cobalt supports key metabolic processes, and its complexes exhibit antioxidant, antibacterial, antifungal, and antiviral properties [22, 23]. Their growing anticancer potential stems from their redox-mediated generation of reactive oxygen species (ROS) and their ability to disrupt DNA, proteins, and cellular pathways, which are finely tuned by coordination geometry and ligand design [14].

Cobalt complexes with carboxylic acid ligands are promising anticancer candidates owing to their structural tunability, favorable redox chemistry, and biocompatibility [24, 25]. The versatile coordination modes of carboxylate ligands influence the electronic environment of the cobalt center, thereby enhancing stability and solubility and enabling controlled Co(II)/Co(III) redox cycling that generates cytotoxic ROS in cancer cells [8, 9, 21]. The resulting oxidative stress triggers mitochondrial damage and apoptosis, positioning these complexes as viable alternatives to platinum drugs [8, 9, 21, 25, 26]. Furthermore, their low toxicity enhances cellular uptake and tumor selectivity [24, 25], and robust carboxylate frameworks can also be engineered to serve as drug-delivery platforms.

Considering the broad significance of carboxylate complexes and their diverse applications, our group is actively involved in the synthesis, properties, structural investigation, and evaluation of carboxylic acid–based metal complexes [26–32]. Herein, we describe a novel Co(II) complex, designated as $[Co(L)(bipy)(H_2O)_2]_n$ (**1**), synthesized through the reaction of cobalt(II) acetate tetrahydrate with 2-((2′-carboxybenzyl)oxy)benzoic acid (H_2L) and 2,2′-bipyridine (bipy) in a 3:1 ethanol and water mixture. The structure and physicochemical properties of the complex (**1**) were thoroughly investigated using elemental analysis (EA), infrared (IR) and ultraviolet–visible (UV–Vis) spectroscopy, thermogravimetric analysis (TG), and single-crystal X-ray diffraction. The electrochemical properties of the complex (**1**) were investigated in acetonitrile and 1.0 $mol{\cdot}L^{-1}$ sulfuric acid solutions. Density functional theory (DFT) calculations were performed to gain deeper insight into the electronic structure, revealing that the HOMO is mainly localized on

the oxygen and nitrogen atoms coordinated to the Co(II) center, while the LUMO is predominantly distributed over the adjacent six-membered aromatic ring. Furthermore, the anticancer effects of the complex (**1**) and $CoCl_2$ were assessed against hepatocyte (L02), pancreatic cancer (PANC-1), and breast cancer (MCF7) cell lines by the MTT assay.

Results and discussion

Infrared spectra

The IR spectra of 2-((2'-carboxybenzyl)oxy)benzoic acid (H_2L) and the complex (**1**) are shown in Fig. 1. The characteristic carboxyl groups bands of 2-((2'-carboxybenzyl)oxy)benzoic acid (H_2L) ligand appear at 1691 cm^{-1} and 1602 cm^{-1}, assigning to the $\nu_{as}COO^-$ and ν_sCOO^-. However, these bands shift to 1597 and 1379 cm^{-1}, respectively, in the complex (**1**), revealing that the carboxylate O atoms of 2-((2'-carboxybenzyl)oxy)benzoic acid (H_2L) ligand are coordination with Co(II) ion [33]. The value of $\Delta\nu$ [$\Delta\nu = \nu_{as}(COO^-)-\nu_s(COO^-)$] is 218 cm^{-1}, suggesting that the carboxylate O atoms of L ligand are coordination with Co(II) ion as monodentate chelate [34–36]. Meanwhile, the C = N absorption peak of the 2,2'-bipyridine appears at 1443 cm^{-1} in the infrared spectrum of the complex (**1**), indicating that the N atoms are also coordination with Co(II) ion [33]. The ν(OH) absorption band around 3082 cm^{-1} confirmes the presence of water molecules in the complex (**1**), consistent with results of thermogravimetric analysis and X-ray single-crystal analysis.

UV-Vis spectra

Figure 2 shows the UV-Vis spectra of 2-((2'-carboxybenzyl)oxy)benzoic acid (H_2L) and the complex (**1**) recorded in aqueous solution ($c = 1.00 \times 10^{-4}$ mol·L^{-1}). The 2-((2'-carboxybenzyl)oxy)benzoic acid (H_2L) exhibits two strong absorption peaks at 196 nm and 233 nm, along with a weak absorption peak around 278 nm, which may be due to the π-π* transitions of the L ligand. The Co(II) complex also exhibits two strong absorption peaks at 195 nm and 231 nm, along a weak, broad absorption peak at approximately 293 nm. The strongest π-π* absorption peak of 2,2'-bipyridine (bipy) appears at 303 nm [37, 38]. The absorption peak at 293 nm in the UV spectrum of the complex (**1**) is attributed to the π-π* absorption peaks of both L and 2,2'-bipyridine (bipy) ligands. For 2,2' -bipiridine (bipy) ligand, the peak shifts to lower wavenumbers due to coordination with Co(II) ions, while for L ligand, the peak shifts to higher wavenumbers under the same coordination, suggesting that both L and bipy ligands are coordinated to the Co(II) ion.

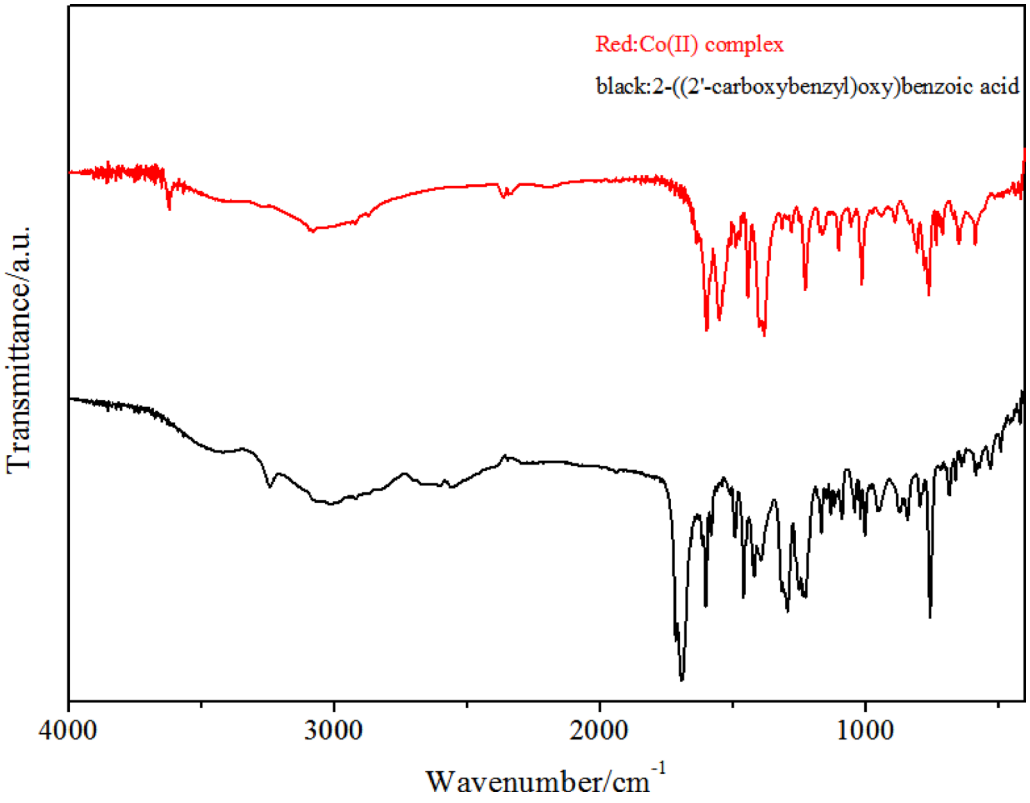

Fig. 1 The IR spectra of 2-((2'-carboxybenzyl)oxy)benzoic acid (H_2L) and the complex (**1**)

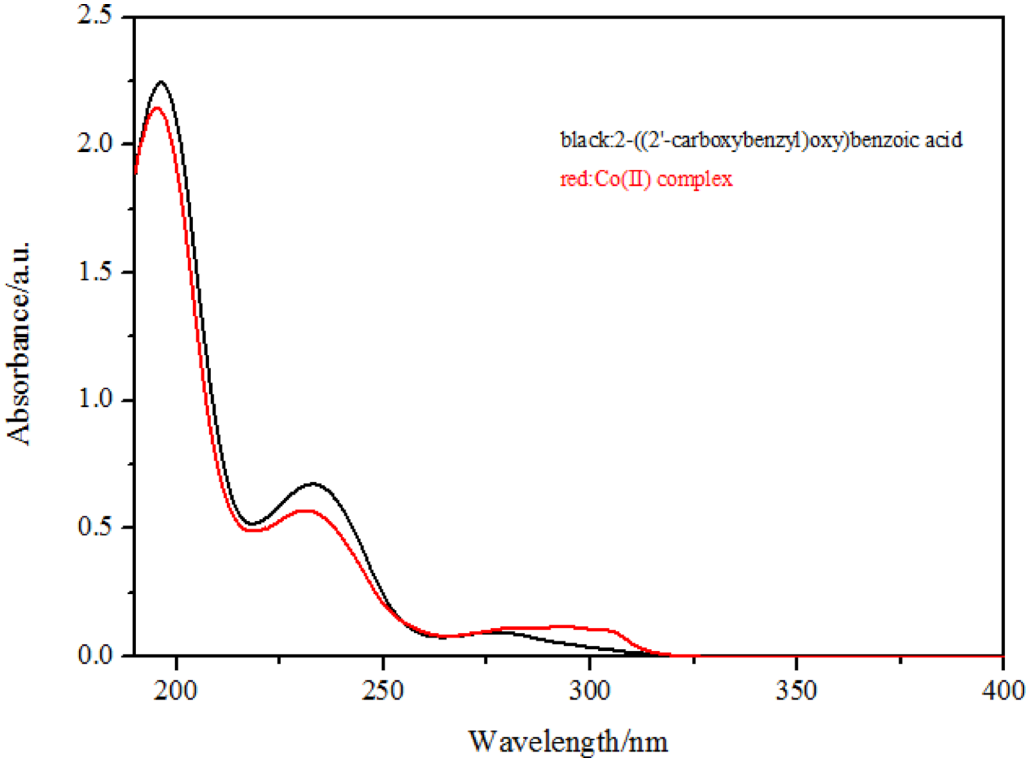

Fig. 2 The UV-Vis spectra of 2-((2′-carboxybenzyl)oxy)benzoic acid (H_2L) and the complex (**1**) in aqueous solution ($c = 1.00 \times 10^{-4}$ mol·L^{-1})

Structural description of the complex (1)

Structural analysis indicates that the complex (**1**) crystallizes in the monoclinic crystal system with space group *C*2/*c*. As shown in Fig. 3, the asymmetric structural unit contains one crystallographically independent Co(II) center, one 2-((2'-carboxybenzyl)oxy)benzoate ligand, one 2,2′-bipyridine (bipy) ligand, and two coordinated water molecules. The Co(II) ion exhibits a six-coordinated geometry, coordinated by two nitrogen atoms (N1, N2) from the chelating 2,2' -bipiridine (bipy) ligand, two oxygen atoms (O1a, O2) from two symmetry-related carboxylate ligands, and two oxygen atoms (O3, O4) from two coordinated water molecules, forming a distorted octahedral environment. In the equatorial plane, the 2-((2'-carboxybenzyl)oxy)benzoate ligand bonds through O1a and O2, while the 2,2' -bipiridine (bipy) ligand coordinates through two nitrogen atoms (N1 and N2). The axial positions are occupied by two water molecules (O3, O4). The selected bond lengths (Å) and bond angles (°) are summarized in Table 1. The Co-O and Co-N bond lengths fall in the ranges from 2.0476(17) to 2.1870(16) Å and from 2.137(2) to 2.1460(19) Å, respectively [Co1-O1a = 2.0802(17) Å, Co1-O2 = 2.0476(17) Å, Co1-O3 = 2.1532(18) Å, Co1-O4 = 2.1870(16) Å, Co1-N1 = 2.1460(19) Å, and Co1-N2 = 2.137(2) Å]. These values are consistent with those reported for related Co(II) complexes in the literature [39–41]. The coordination environment around the Co(II) center is further characterized by bond angles, including O1a-Co1-N1 = 90.66(7)°, O2-Co1-O1a = 101.55(7)°, O2-Co1-N2 = 94.46(8)°, N1-Co1-N2 = 75.45(8)°, and O3-Co1-O4 = 168.35(7)°, which indicate a distorted octahedral geometry. The dihedral angle of two benzene rings of 2-((2'-carboxybenzyl)oxy)benzoate ligand is 82.96°, demonstrating that the complex (**1**) adopts a markedly non-coplanar conformation. Notably, the oxygen atoms of the two carboxylate groups coordinate to distinct Co(II) centers, thereby forming one-dimensional zigzag coordination chains (Fig. 4). These chains are further assembled into a two-dimensional supramolecular architecture through π–π stacking interactions between adjacent 2,2′-bipyridine rings, with an average centroid–centroid separation of 3.373 Å (Fig. 5). In addition, intermolecular hydrogen-bonding interactions between carboxylate oxygen atoms and coordinated water molecules significantly stabilize the overall crystal structure (Table 2).

DFT calculations

Density functional theory (DFT) calculations were performed to provide a deeper understanding of the electronic structure of the complex (**1**). Electrostatic potential (ESP) mapping and frontier molecular orbital (FMO) analyses were conducted using the DMol^3 module in Materials Studio 2020. The DFT results reveal that the highest occupied molecular orbitals (HOMO) (-0.211 Ha (-5.741 eV)) are primarily localized on the oxygen

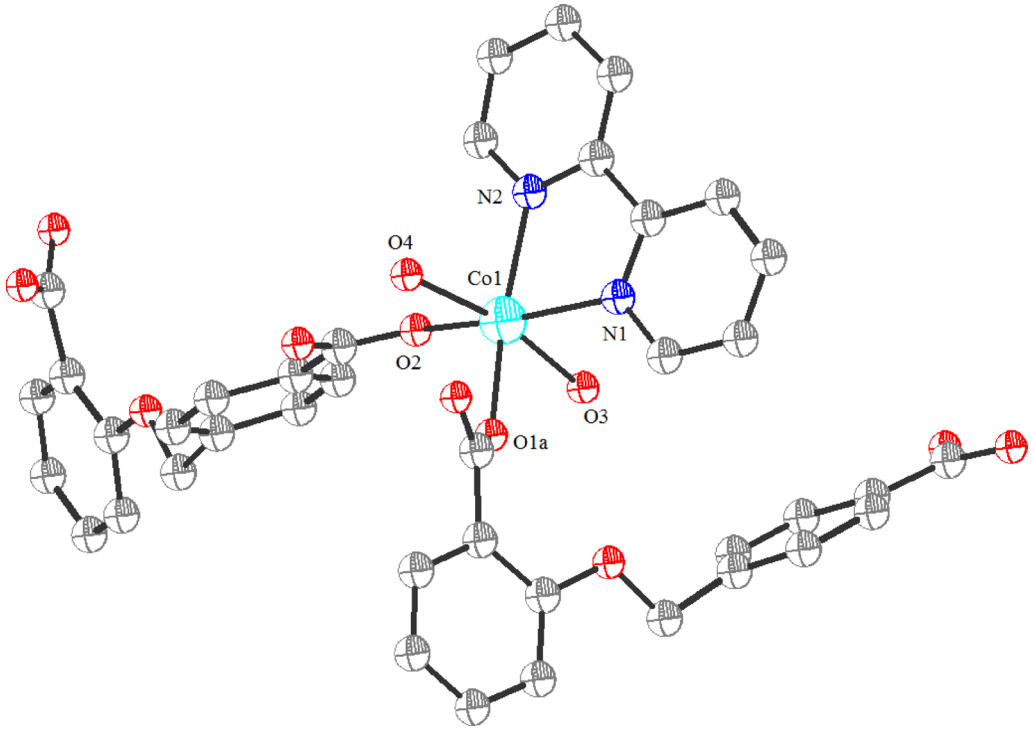

Fig. 3 The coordination environment of Co(II) ion. Symmetric operation code: a: *x*, 1-*y*, 1/2 + *z*

Table 1 Selected bond lengths (Å) and bond angles (°) for the complex (**1**)

Bond	d	Angle	(°)
Co1-O1a	2.0802(17)	O1a-Co1-O3	83.99(7)
Co1-O2	2.0476(17)	O1a-Co1-O4	87.29(6)
Co1-O3	2.1532(18)	O1a-Co1-N1	90.66(7)
Co1-O4	2.1870(16)	N2-Co1-O1a	162.56(8)
Co1-N1	2.1460(19)	O2-Co1-O1a	101.55(7)
Co1-N2	2.137(2)	O2-Co1-O3	85.42(7)
		O2-Co1-O4	88.77(7)
		O2-Co1-N1	162.27(8)
		O2-Co1-N2	94.46(8)
		O3-Co1-O4	168.35(7)
		N1-Co1-O3	83.11(7)
		N1-Co1-O4	104.76(7)
		N2-Co1-O3	104.33(8)
		N2-Co1-O4	86.17(7)
		N2-Co1-N1	75.45(8)

Symmetric operation code: a: *x*, 1-*y*, 1/2 + *z*

and nitrogen donor atoms coordinated to the Co(II) ion, while the lowest unoccupied molecular orbitals (-0.15402 Ha (-4.191 eV)) are mainly situated on the adjacent six-membered aromatic carbon ring (Fig. 6). Furthermore, the ESP analysis reveals regions of higher electrostatic potential concentrated on the six-membered carbon ring, whereas regions of lower potential are predominantly associated with the oxygen and nitrogen atoms (Fig. 7), suggesting electrophilic and nucleophilic interaction sites, respectively.

Electrochemical activity

To better understand the electrochemical properties of the complex (**1**), cyclic voltammetry (CV) was conducted in acetonitrile (ACN) with tetrabutylammonium tetrafluoroborate (TBATFB) as the supporting electrolyte. The experiments were carried out under a nitrogen atmosphere using a CS310M electrochemical analyzer in a standard three-electrode configuration: a working electrode consisting of the complex (**1**) coated on an indium tin oxide (ITO) substrate, an Ag/AgCl reference electrode, and a platinum wire counter electrode. As shown in Fig. 8A, the complex (**1**) exhibits a well-defined redox behavior between 1.0 and 2.0 V, attributable to the Co(III)/Co(II) redox process. The nearly symmetrical anodic and cathodic peaks indicate that the electron-transfer process is predominantly reversible, demonstrating good electrochemical stability of the complex under the experimental conditions.

To investigate the electrochemical behavior of the complex (**1**) in an acidic environment, cyclic voltammetry measurements were performed in 1 mol·L^{-1} sulfuric acid solution. As shown in Fig. 8B, the complex (**1**) exhibits a pronounced redox response under acidic conditions. Unlike the reversible Co(III)/Co(II) couple observed in ACN/TBATFB, the CV in H_2SO_4 shows a continuous increase in current density during the anodic scan across

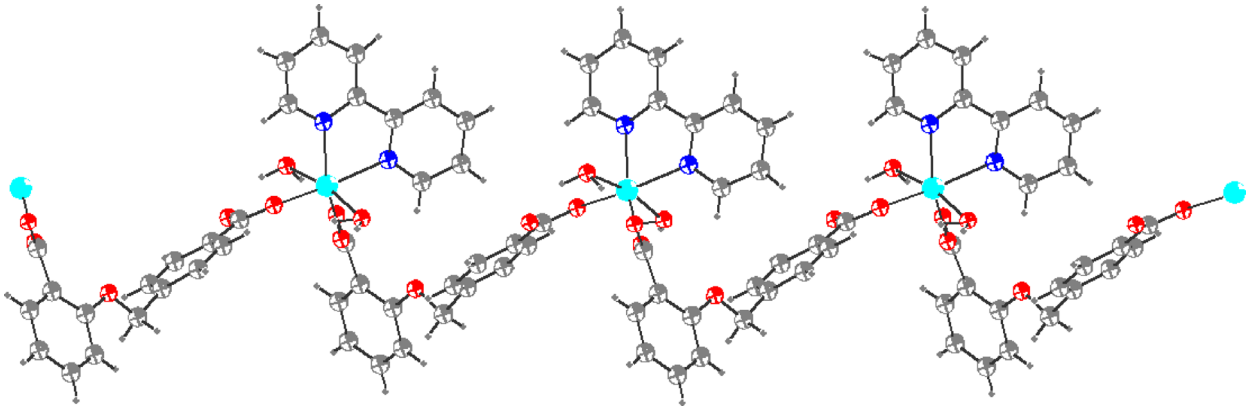

Fig. 4 One-dimensional zigzag chains structure of the complex (**1**)

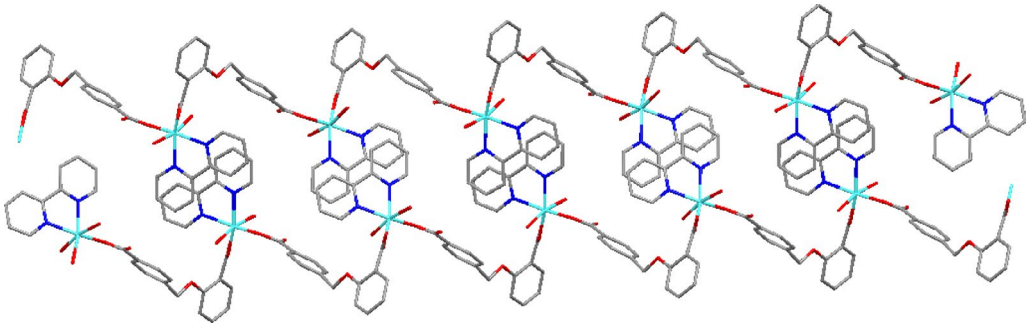

Fig. 5 Three-dimensional network structure of the complex (**1**)

Table 2 Hydrogen bonds in the Co(II) complex

Donor-H	Acceptor	D-H (Å)	H···A (Å)	D···A (Å)	D-H···A (°)	Symmetric operation
O3-H3A	O6	0.86	1.95	2.697(2)	144	1/2-*x*, 1/2-*y*, -*z*.
O4-H4A	O7	0.86	1.89	2.655(2)	148	
O4-H4B	O1	0.86	2.51	2.946(3)	112	*x*, *y*, *z*
O4-H4B	O6	0.86	1.84	2.689(3)	171	*x*, *y*, *z*

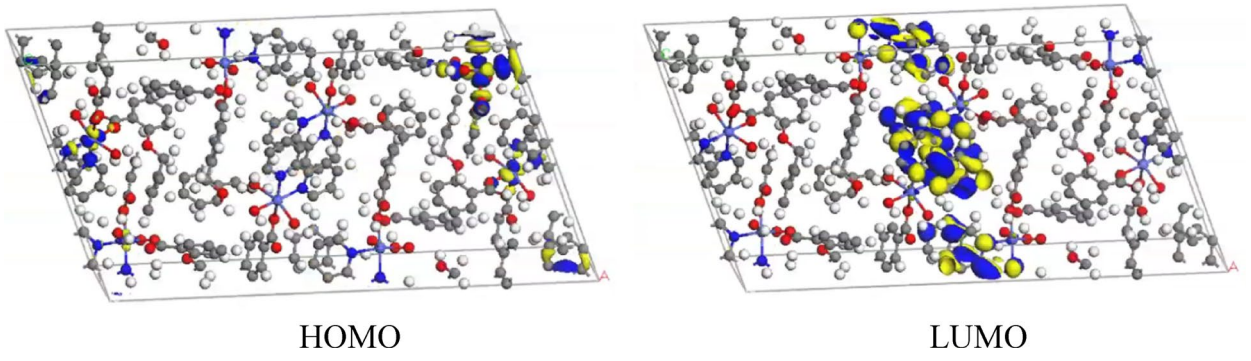

Fig. 6 The frontier molecular orbitals of the complex (**1**)

the potential range of 0–1.0 V, featuring a distinct oxidation peak centered at around 0.3 V. This behavior is likely attributable to the protonation of the ligand moieties in the acidic environment, which significantly affects the complex's electron-transfer properties. Therefore, the overall redox activity in 1 mol·L^{-1} H_2SO_4 involves both ligand protonation-oxidation processes and the metal-centered Co(III)/Co(II) redox couple.

Thermogravimetric analysis

Thermogravimetric analysis (TGA) was conducted to assess the thermal stability of the complex (**1**) in an air

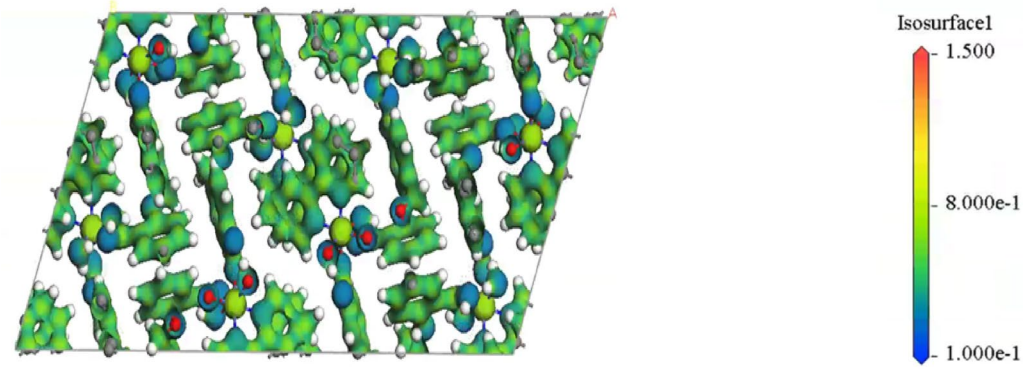

Fig. 7 Electrostatic potential of the complex (**1**)

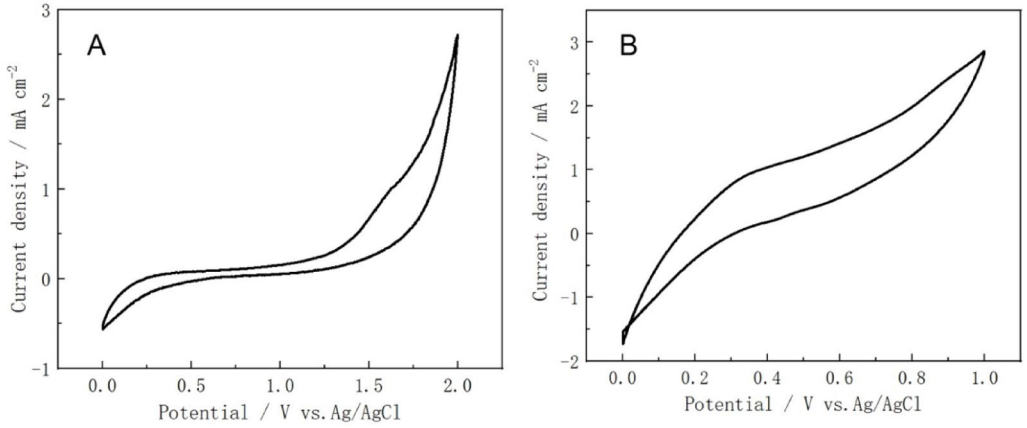

Fig. 8 CV curve of the complex (**1**) in ACN using TBATFB as the supporting electrolyte (**A**) and 1 mol·L^{-1} sulfuric acid solution (**B**)

atmosphere at a heating rate of 10 °C min^{-1} across a temperature range of 25–650 °C (Fig. 9). The TGA profile shows an initial weight loss between 25 and 105 °C, due to the desorption of physically adsorbed water molecules. The initial mass loss of 6.81% (calculated: 6.91%) observed between 25 and 105 °C is attributable to the release of two coordinated water molecules. The experimentally observed mass loss (6.81%) is close to the theoretically calculated value of 6.91%. Upon further heating, the complex (**1**) remains relatively stable up to approximately 280 °C, beyond which the coordination framework decomposes gradually in the temperature range 280–440 °C. The maximum rate of weight loss occurs at approximately 440 °C, corresponding to an overall mass loss of 87.1%. The residual mass accounted for 12.9% of the initial mass, consistent with the formation of CoO, which has a theoretical residue of 14.39%.

Cytotoxic effects

Long-term exposure to cobalt environments may lead to potential cobalt toxicity, cardiotoxicity, or carcinogenicity. This occurs because cobalt ions can induce the production of reactive oxygen species (ROS). Consequently, researchers are increasingly exploring the development of anticancer drugs based on cobalt's toxic properties [42]. To examine the changes in cobalt ion properties after coordination, the normal hepatocyte cell line L02, pancreatic cancer cell line PANC-1, and breast cancer cell line MCF7 were used to assess the cytotoxicity of the complex (**1**) and free Co^{2+}. Considering the differences in molecular weight and cobalt concentration between the two substances, the experimental IC_{50} values were converted based on cobalt content. As shown in Fig. 10, the IC_{50} values of the complex (**1**) and $CoCl_2$ against L02 cells were 21.4587 μg/mL and 42.8521 μg/mL, respectively; for PANC-1 and MCF7 cells, the values were 16.1929 μg/mL, 25.7608 μg/mL, and 15.1872 μg/mL, 28.7827 μg/mL. Both substances exhibited cytotoxic effects on normal cells and cancer cells; however, the IC_{50} values for the two cancer cell lines were lower than those for normal cells across various treatments. Therefore, cancer cells are more sensitive to cobalt-containing substances. The IC_{50} value of the complex (**1**) is significantly lower than that of cobalt chloride, which means that at the same cobalt concentration, the complex (**1**) exhibits nearly twice the toxicity to cells compared to cobalt chloride.

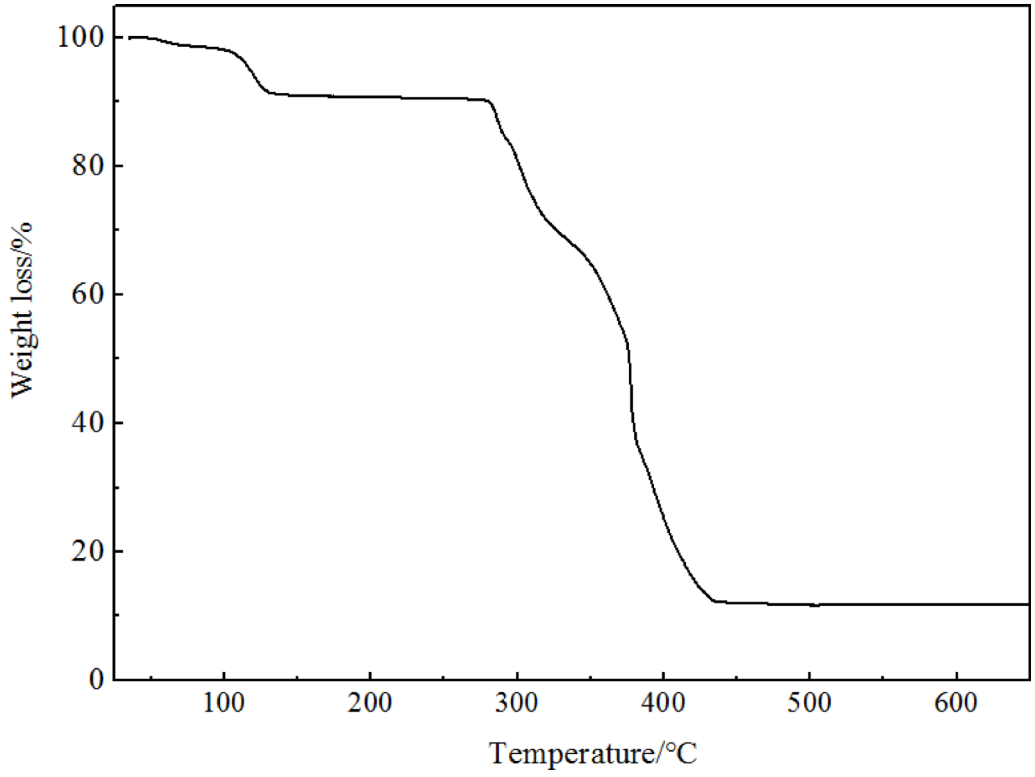

Fig. 9 Thermogravimetric curve of the complex (**1**)

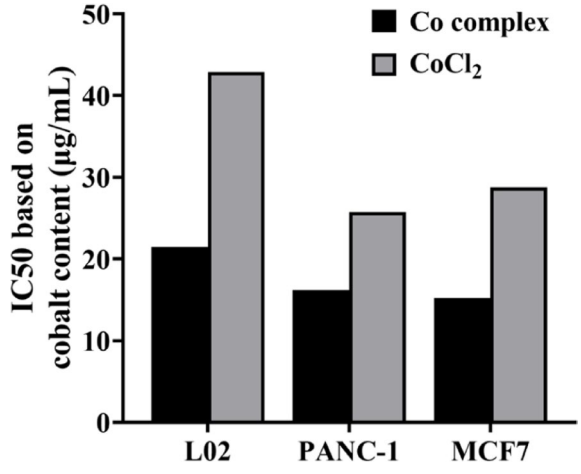

Fig. 10 The comparison of IC50 of the complex (**1**) and $CoCl_2$ for L02, PANC-1 and MCF7 cells

This phenomenon is due to the high metabolic activity of cancer cells, which facilitates faster cobalt absorption, as well as the naturally higher accumulation of reactive oxygen species (ROS) in these cells [43, 44]. When comparing the effects of the complex (**1**) and $CoCl_2$ treatments, the complex (**1**) exhibited lower IC_{50} values in all three cell lines, indicating higher cytotoxicity at the same cobalt concentration. This benefit arises from the negative charge of the carboxyl groups in the ligand, which increases the affinity of the complex (**1**) for biological membranes [45]. Additionally, the presence of 2,2'-bipyridyl increases the lipophilicity of Co(Ⅱ) ions, facilitating their translocation across cell membranes, whereas free Co(Ⅱ) ions primarily enter cells through protein-mediated transport or endocytosis [46].

Notably, low concentrations of $CoCl_2$ had a significant proliferative effect on cells. Compared to the untreated control, low-concentration $CoCl_2$ increased L02 cell viability to 101.28% (Fig. 11), and PANC-1 and MCF7 cell viabilities to 108.99% (Fig. 12) and 110.04% (Fig. 13), respectively. The proliferative effect was more significant in cancer cells than in normal cells. However, this effect was not seen in the complex (**1**) treatment groups (Figs. 11, 12 and 13). This might be because low concentrations of free Co(Ⅱ) ions support normal cellular physiological functions. Furthermore, $CoCl_2$ has been shown to act as a deoxygenating agent that simulates the hypoxic tumor microenvironment, and specific concentrations of $CoCl_2$ may promote cancer cell proliferation [47, 48]. In contrast, after binding to the ligand, Co(Ⅱ) ions can no longer interact normally with relevant proteins, preventing them from carrying out their physiological functions, which clarifies that the complex (**1**) does not induce cell growth.

Additionally, the IC_{50} values of the complex (**1**) against the two cancer cell lines were similar, indicating that the complex (**1**) works through the same anticancer

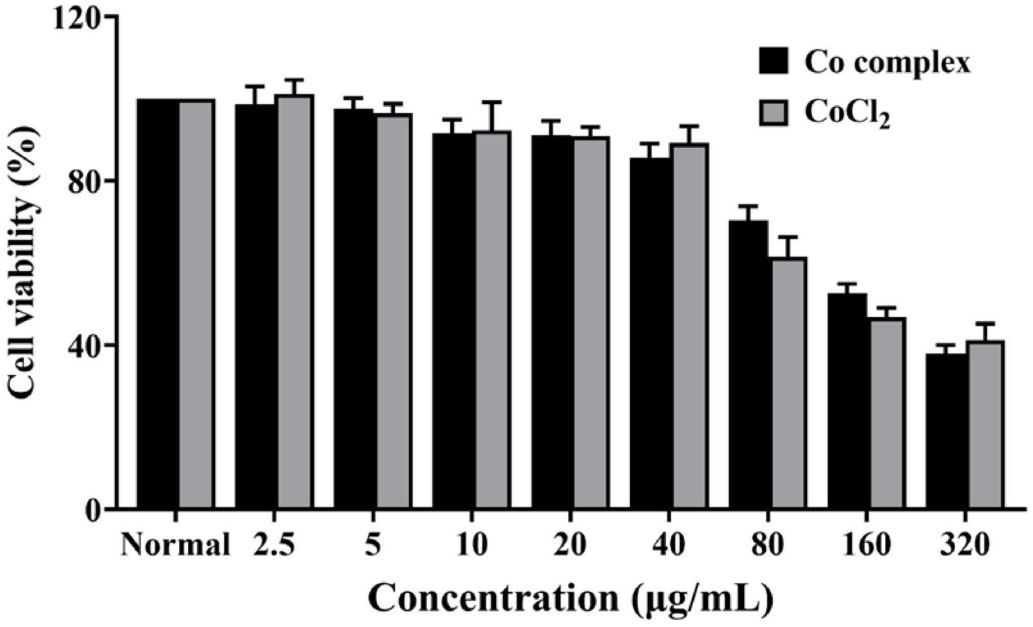

Fig. 11 The comparison of the viability of L02 cells treated with the complex (**1**) and $CoCl_2$ at gradient concentrations by MTT assay

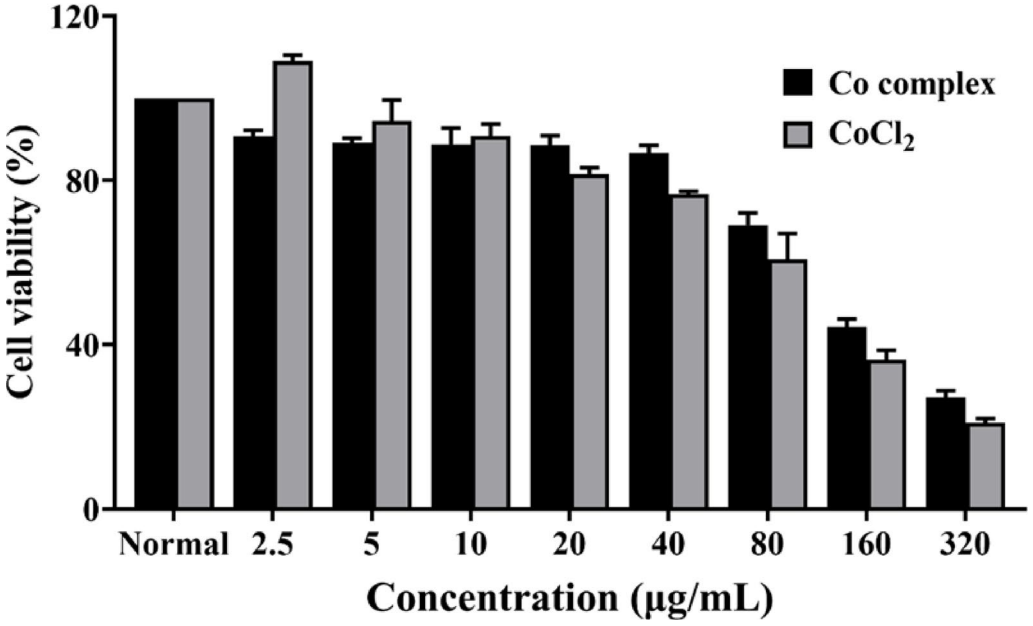

Fig. 12 The comparison of viability of PANC-1 cells treated with the complex (**1**) and $CoCl_2$ at gradient concentrations by MTT assay

mechanism—namely, oxidative stress caused by excessive ROS production—in eliminating both cancer cell types. In summary, compared with free Co(Ⅱ) ions, the ligand-coordinated Co(Ⅱ) complex exhibits higher selectivity for cancer cells and enhanced anticancer activity. These findings provide insights into the development of more effective cobalt-based anticancer medicines and promote further investigation into the mechanisms of cobalt toxicity.

Experimental

Materials and measurements

Cobalt(II) acetate tetrahydrate, 2-((2'-carboxybenzyl) oxy)benzoic acid (L1), 2,2'-bipyridine (L2), NaOH, and ethanol were received from Jilin Chinese Academy of Sciences-Yanshen Technology Co., Ltd. (Jilin, China). An Elementar Vario III EL elemental analyzer (Elementar, Germany) was used to determine the C, H, and N content. Functional group identification was conducted using a Tianjin Gangdong FTIR-850 spectrophotometer

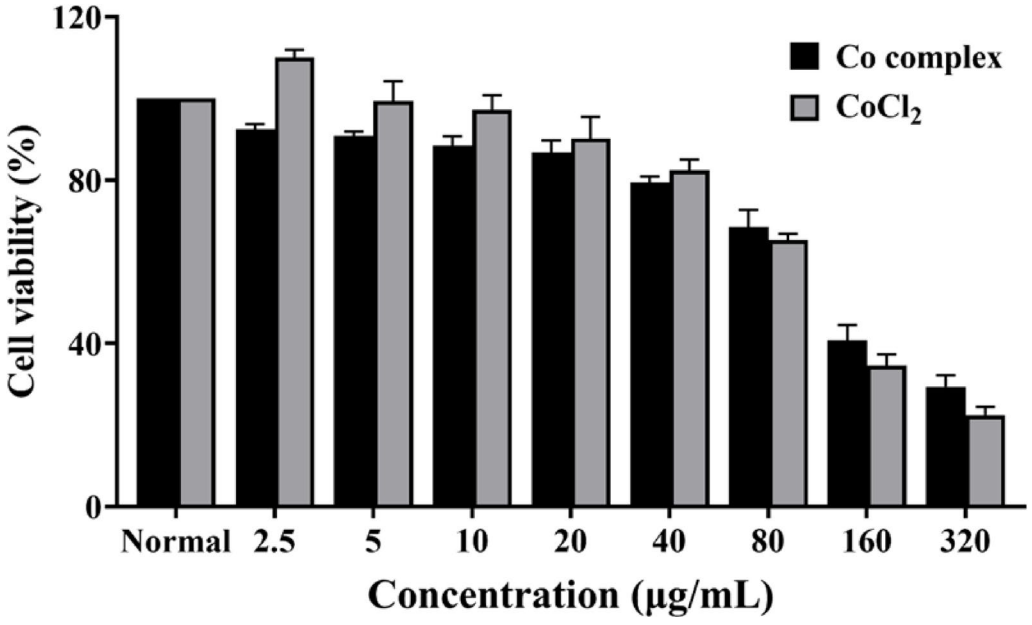

Fig. 13 Comparison of MCF7 cell viability treated with the complex (**1**) and $CoCl_2$ at varying concentrations using MTT assay

Table 3 The crystal structural parameters for the complex (1)

Empirical formula	$C_{25}H_{22}CoN_2O_7$
Formula weight	521.37
Temperature/*K*	296
Crystal system	monoclinic
Space group	*C2/c*
a/Å	35.1057(18)
b/Å	7.2928(3)
c/Å	19.1436(9)
β/°	109.990(2)
Volume/Å^3	4605.8(4)
Z	8
ρ_{calc}, mg/mm^3	1.504
μ/mm^{-1}	0.795
S	1.220
F(000)	2152
Index ranges	$-41 \le h \le 41$, $-8 \le k \le 8$, $-22 \le l \le 22$
Reflections collected	29,833
Independent reflections	3970 [R(int) = 0.0543]
Data/restraints/parameters	3970/0/312
Goodness-of-fit on F^2	1.220
Refinement method	Full-matrix least-squares on F^2
Final *R* indexes [$I >= 2\sigma(I)$]	$R_1 = 0.0399$, $wR_2 = 0.0983$
Final *R* indexes [all data]	$R_1 = 0.0462$, $wR_2 = 0.1025$

(Tianjin, China) with KBr pellets, covering the range of 4000–400 cm^{-1}. UV-Vis spectra were recorded from 190 to 700 nm using a PERSEE T9 spectrophotometer (Beijing, China). Thermal stability was examined with a HENVEN HCT-2 thermal analyzer (Beijing, China). The crystal structure was analyzed with a Bruker CCD area detector (SuperNova, Billerica, MA, USA).

Synthesis of the complex (1)

0.1360 g of 2-((2'-Carboxybenzyl)oxy)benzoic acid (0.5 mmol) and 0.040 g NaOH (1.0 mmol) were dissolved in a solvent mixture consisting of 10 mL of ethanol and 5 mL water. Subsequently, 0.1245 g of cobalt(II) acetate tetrahydrate (0.5 mmol) solid was added to the above solution while stirring. The reaction mixture was stirred at 78 °C for 1 h, then 5 mL ethanol solution containing 0.0781 g of 2,2'-bipyridine (0.5 mmol) was added. The solution was stirred again at 78 °C for another 3 h, then cooled to room temperature and filtered. The block crystals formed after 21 days.

Crystal structure determination

The block crystals (0.18 mm×0.15 mm×0.13 mm) were selected and mounted on the Bruker Smart CCD X-ray single-crystal diffractometer. The diffractometer was equipped with Mo *Kα* monochromatic X-ray (λ = 0.071073 nm) and the *ω*-scans mode was used to collect the diffractogram of the complex (**1**) at 296 K. The collected data were corrected for absorption using Olex2 [49], and the direct method was applied to solve the structure using SHELXS [50]. The detailed crystallographic parameters are summarized in Table 3.

Cell culture

The normal liver cell line L02 and cancer cells lines PANC-1 and MCF7 were obtained from the National Collection of Authenticated Cell Cultures. They were

cultured using DMEM or RPMI-1640 medium, respectively, supplemented with 10% fetal bovine serum (FBS, HyClone), 100 U/mL penicillin, and 100 μg/mL streptomycin. Cells were maintained in a cell culture incubator at 37℃ and 5% CO_2. For the methylthiazolyldiphenyltetrazolium bromide (MTT) assay, digested cells were plated on 96-well plates and cultured for at least 24 h to reach approximately 50–60% confluence.

MTT assay

The MTT assay was performed according to the Beyotime manual (ST316) with some modifications. The L02, PANC-1 or MCF7 cells suspensions were plated onto 96-well plates (100 μl per well). The perimeter wells (rows A and H; columns 1 and 12) were filled with PBS to prevent edge effects (evaporation). The cell columns were treated with a gradient concentration of the complex (**1**) or cobalt chloride hexahydrate (0 ~ 320 μg/mL) overnight at 37℃. After treatment, 10 μL of MTT solution (5 mg/mL) was added to each well. Following 4 h of incubation, the solution in the wells was discarded, and 100 μL of DMSO was added to dissolve the formed formazan. The optical density (OD) was measured using a microplate reader at a wavelength of 490 nm.

Conclusions

In conclusion, a novel Co(II) complex was successfully synthesized and structurally characterized, revealing a distorted octahedral [CoO_4N_2] geometry and a 2D layered architecture mediated by π-π interactions. DFT and electrostatic analyses provided insight into electronic distribution. Cyclic voltammetry studies revealed medium-dependent redox behavior, with reversible Co(III)/Co(II) processes in ACN and ligand-influenced oxidation in acidic media, highlighting the complex's pH-sensitive redox activity and potential for diverse electrochemical environments. Biological evaluation showed that the complex exhibits enhanced cytotoxicity and selectivity for cancer cells compared with free Co^{2+}, without promoting cell proliferation at low concentrations, highlighting its potential as a cobalt-based anticancer agent.

Supplementary Information

The online version contains supplementary material available at https://doi.org/10.1186/s13065-026-01743-y.

Supplementary Material 1.

Supplementary Material 2.

Author contributions

Sui B.L.: Conceptualization, methodology, investigation, resources, data curation, writing-original draft, review, and editing; Tai X.S and Wang L.H.: Investigation, resources, writing, review, and editing, validation; Azam M. and Al-Resayes S.I.: Writing-review and extensive editing; Wang A.L.: Data curation, writing-review and editing. All authors have read and agreed to the manuscript.

Funding

This project was supported by the National Natural Science Foundation of China (No. 21171132), the Science Foundation of Weifang (2020ZJ1054), and the Science Foundation of Weiyuan Scholars Innovation Team. The authors acknowledge the financial support from the Ongoing Research Funding Program, (ORF-2025-147), King Saud University, Riyadh, Saudi Arabia.

Data availability

The crystallographic data for the structure described have been deposited with the Cambridge Crystallographic Data Centre under the supplementary publication number CCDC 2478046. The corresponding CIF file can be easily accessed through the website: https://www.ccdc.cam.ac.uk/structures.

Declarations

Ethics approval and consent to participate

Not applicable.

Consent for publication

Not applicable.

Competing interests

The authors declare no competing interests.

Author details

[1]College of Chemistry and Chemical Engineering, Weifang University, Weifang 261061, P. R. China
[2]College of Biology and Oceanography, Weifang University, Weifang 261061, P. R. China
[3]Department of Chemistry, College of Science, King Saud University, PO BOX 2455, Riyadh 11451, Saudi Arabia
[4]Affiliated Beijing Chaoyang Hospital, Capital Medical University, No. 8 Gongren Tiyuchang Nanlu, Chaoyang District, Beijing 100020, PR China

Received: 9 December 2025 / Accepted: 27 January 2026
Published online: 05 February 2026

References

1. Sun M, Fan WD, Wang XK, Gao F, Liu XP, Han YF, Kang ZX, Meng QG, Sun DF. Isoreticular expansion of UiO-66 via vinyl for efficient C_2H_2/CO_2 separation. Sep Purif Technol. 2025;361:131342.
2. Xu MM, Li Y, Wang XK, Liu HY, Liu QR, Zhang YF, Fan WD, Meng QG, Sun DF. Imidazole-functionalized Zn-MOFs for one-step C_2H_4 purification from $C_2H_2/C_2H_4/C_2H_6$ ternary mixture. Inorg Chem. 2025;64:813–7.
3. Constable EC, Parkin G, Que L, editors. Comprehensive coordination chemistry III. Elsevier; 2021.
4. Panova EV, Voronina JK, Azizova AN, Tutar OF, Mahmoudi G, Safinm DA. Heteroleptic cobalt(II) coordination compounds fabricated from the CoX_2 ($X = NO_3^-, Cl^-$) salts, benzoic acid and polypyridines (1,10-phenanthroline, 2,2′-bipyridine). J Mol Struct. 2026;1352:144040.
5. Kyne SH, Lef`evre G, Ollivier C, Petit M, Ramis Cladera V-A, Fensterbank L. Iron and Cobalt catalysis: new perspectives in synthetic radical chemistry. Chem Soc Rev. 2020;49:8501–42.
6. Murrie M. Cobalt(II) single-molecule magnets. Chem Soc Rev. 2010;39:1986–95.
7. Droghetti F, Lucarini F, Molinari A, Ruggi A, Natali M. Recent findings and future directions in photosynthetic hydrogen evolution using polypyridine Cobalt complexes. Dalton Trans. 2022;51:10658–73.
8. Cressey P, Eskandari A, Bruno P, Lu C, Hemann M, Suntharalingam K. The potent inhibitory effect of a naproxen-appended cobalt(III)-cyclam complex on cancer stem cells. ChemBioChem. 2016;17:1713–8.
9. Fang J, Orobator ON, Olelewe C, Passeri G, Singh K, Awuah SG, Suntharalingam K. A breast cancer stem active cobalt(III)-cyclam complex containing flufenamic acid with Immunogenic potential. Angew Chem Int Ed. 2024;63:e202317940.
10. Gu J, Wen M, Liang X, Shi Z, Kirillova MV, Kirillov AM. Multifunctional aromatic carboxylic acids as versatile Building blocks for hydrothermal design of coordination polymers. Crystals. 2018;8:83.

11. Zhou HC, Long JR, Yaghi OM. Introduction to metal-organic frameworks. Chem Rev. 2012;112:673–4.
12. Lee J, Farha OK, Roberts J, Scheidt KA, Nguyen ST, Hupp JT. Metal-organic framework materials as catalysts. Chem Soc Rev. 2009;38:1450–9.
13. Lu H, Fu D, Tai XS, Sun ZL, Wang XK. Metal-organic frameworks/covalent-organic frameworks-based materials in organic/inorganic pollutant elimination and CO_2 reduction applications, chemnanomat. (2025)e202500244.
14. Renfrew AK, O'Neill ES, Hambley TW, New EJ. Harnessing the properties of Cobalt coordination complexes for biological application. Coord Chem Rev. 2018;375:221–33.
15. Paliwal K, Swain A, Mishra DP, Antharjanam PKS, Kumar M. A novel copper(II) complex with a Salicylidene carbohydrazide ligand that promotes oxidative stress and apoptosis in triple negative breast cancer cells. Dalton Trans. 2024;53:17702–20.
16. Bosl GJ, Motzer RJ. Testicular germ-cell cancer, N. Engl. J Med. 1997;337:242–53.
17. Jung Y, Lippard SJ. Direct cellular responses to platinum-induced DNA damage. Chem Rev. 2007;107:1387–407.
18. Sharma H, Pathak M. Synthesis and theoretical evaluation of new copper(II) complexes associated with a crystalline schiff base: DNA/BSA protein interaction, radical scavenging and cytotoxicity. Eur J Inorg Chem. 2024;27:e202400302.
19. Egorova KS, Ananikov VP. Toxicity of metal compounds: knowledge and Myths. Organometallics. 2017;36:4071–90.
20. Droghetti F, Lucarini F, Molinari A, Ruggi A, Natali M. Ecent findings and future directions in photosynthetic hydrogen evolution using polypyridine Cobalt complexes. Dalton Trans. 2022;51:10658–73.
21. Shaikh SA, Bhat SS, Hegde PL, Revankar VK, Kate A, Kirtani D, Kumbhar AA, Kumbar V, Bhat K. Synthesis, structural characterization, protein binding, DNA cleavage and anticancer activity of fluorophore labelled copper(II) complexes based on 1,8-naphthalimide conjugates. New J Chem. 2021;45:16319–32.
22. Daumann LJ, Comba P, Larrabee JA, Schenk G, Stranger R, Cavigliasso G, Gahan LR. Synthesis, magnetic properties, and phosphoesterase activity of dinuclear cobalt(II) complexes. Inorg Chem. 2013;52:2029–43.
23. Dwyer FP, Gyarfas EC, Rogers WP, Koch JH. Biological activity of complex ions. Nature. 1952;170:190–1.
24. Bilal H, Zahoor S, Choudhary MI, Shaheen F, Dejadisai S, Liang H, Chen ZF. Carboxylate embedded metal organic frameworks for potential applications in drug delivery and controlled release. Coord Chem Rev. 2025;538:216688.
25. Devereux M, McCann M, Leon V, Geraghty M, McKee V, Wikaira J. Synthesis and fungitoxic activity of manganese(II) complexes of fumaric acid: X-ray crystal structures of [Mn(fum)(bipy)(H_2O)] and [Mn(Phen)$_2$(H_2O)$_2$](fum)·4H_2O (fumH_2=fumaric acid; bipy = 2,2′-bipyridine; phen = 1,10-phenanthroline). Polyhedron. 2000;19:1205–11.
26. Wang LH, Tai XS. Synthesis, structural characterization, Hirschfeld surface analysis and photocatalytic CO_2 reduction activity of a new dinuclear Gd(III) complex with 6-phenylpyridine-2-carboxylic acid and 1,10-phenanthroline ligands. Molecules. 2023;28:7595.
27. Tai XS, Wang LH, Al-Resayes SI, Azam M. Synthesis, structural characterization, Hirschfeld surface analysis and catalytic application of a new cd(II) complex bearing 1H-pyrazolo[3,4-b] pyridine-3-amine and pyridine carboxylic acid. Polyhedron. 2025;279:117647.
28. Wang LH, Tai XS, Azam M, Sui BL, Wang AL. Synthesis, structural characterization, and Hirschfeld surface analysis of a novel Mn(II) complex based on N-acetyl-L-phenylalanine ligand and its evaluation as a cytotoxic agent. Polyhedron. 2025;279:117659.
29. Tai XS, Yan XH, Wang LH. Synthesis, structural characterization, Hirschfeld surface analysis, density functional the-ory, and photocatalytic CO_2 reduction activity of a new Ca(II) complex with a bis-Schiff base ligand. Molecules. 2024;29:1047.
30. Cao SH, Tai XS, Xin CL. Synthesis, crystal structure and antitumor activity of a Ca(II) coordination polymer based on 4-acetylphenoxyacetate ligands. Chin J Struct Chem. 2021;40:324–8.
31. Liu P, Wang LH, Tai XS. The crystal structure of catena-poly[bis(6-phenylpyridine-2-carboxylato-κ^{2}N,O)-(μ$_2$-4,4′-bipyridne-κ^{2}N:N)cadmium(II)], $C_{34}H_{24}N_4O_4Cd$, Z. Kristallogr.-N. Cryst Struct. 2023;238:771–3.
32. Zhou XJ, Liu LL, Kou H, Zheng SM, Song MJ, Lu JT, Tai XS. A multifunctional 3D supermolecular Co coordination polymer with potential for CO_2 adsorption, antibacterial activity, and selective sensing of Fe^{3+}/Cr^{3+} ions and TNP. Front Chem. 2021;9:678993.
33. Nakamoto K. Infrared spectra of inorganic and coordination compounds. Interscience, New York: Wiley; 1970.
34. Pirsiavash F, Amani V, Abedi A. Coordination number in copper(II) complexes with bipyridine-dicarboxylate anion and Diamine derivatives. Res Chem Intermed. 2018;44:7411–26.
35. Pour NT, Khalighi A, Yousefi M, Amani V. One-dimensional barium coordination polymer with 2,2′-bipyridine-5,5′-dicarboxylate ligand: synthesis, spectroscopic characterization, thermal analyses, and crystal structure. Synth React Inorg M. 2015;45:1427–33.
36. Amani V, Safari N, Khavasi HR. Solution and solid state characterization of oxo-centered trinuclear iron(III) acetate complexes [Fe_3(μ$_3$-O)(μ-OAc)$_6$(L)$_3$]$^+$, Spectrochim. Acta A. 2012(2012).
37. Lever ABP. Inorganic electronic spectroscopy, 2nd Edn, Elsevier, Amsterdam (1984).
38. Sabeg Y, Benali-Cherif R, Falek W, Takouachet R, Golea L, Aygün M, Benali-Cherif N. Comprehensive study of a novel cobalt(II) complex: Synthesis, X-ray crystal structure, Hirshfeld surface analysis, computational quantum investigations, and molecular Docking insights. Polyhedron. 2025;271:117445.
39. Tai XS, Xia YP. The crystal structure of [(2,2′-bipyridine-k^{2}N,N)-bis(6-phenylpyridine-2-carboxylato-k^{2}N,O)cobalt(II)]-monohydrate, $C_{36}H_{26}N_4O_5Co$, Z. Kristallogr.-N. Cryst Struct. 2022;237:225–7.
40. Gao X, Tai XS. The crystal structure of diaqua-bis(6-phenylpyridine-2-carboxylato-κ^{2}N,O)cobalt(II)-water-N,N-dimethylformamide(1/2/1), $C_{27}H_{31}N_3O_9Co$, Z. Kristallogr.-N. Cryst Struct. 2022;237:393–5.
41. Tai XS, Wang ZJ, Ouyang J, Li YF, Zhang W, Jia WL, Wang LH. The crystal structure of [(phenantroline-κ$_2$N,N′)-bis(6-phenylpyridine-2-carboxylate-k^{2}N,O)cobalt(II)]monohydrate, $C_{36}H_{26}N_4O_5Co$, Z. Kristallogr.-N. Cryst Struct. 2021;236:1309–11.
42. Cai SF, Liu JM, Ding JW, Fu Z, Li HL, Xiong YL, Zeng L, Yang R, Chen CY. Tumor-Microenvironment-Responsive cascade reactions by a Cobalt-Single-Atom nanozyme for synergistic nanocatalytic chemotherapy. Angew Chem Int Ed. 2022;61:e202204502.
43. Ma N, Wang Y, Li X, Xu M, Tan D. Reactive oxygen species in cancer: mechanistic insights and therapeutic innovations. Cell Stress Chaperon. 2025;30:100108.
44. Glorieux C, Liu S, Trachootham D, Huang P. Targeting ROS in cancer: rationale and strategies. Nat Rev Drug Discov. 2024;23:583–606.
45. Shamay Y, Shpirt L, Ashkenasy G, David A. Complexation of cell-penetrating peptide-polymer conjugates with polyanions controls cells uptake of HPMA copolymers and anti-tumor activity. Pharm Res. 2014;31:768–79.
46. Komeda H, Kobayashi M, Shimizu S. A novel transporter involved in Cobalt uptake. Proc Natl Acad Sci. 1997;94:36–41.
47. Rana NK, Singh P, Koch B. CoCl2 simulated hypoxia induce cell proliferation and alter the expression pattern of hypoxia associated genes involved in angiogenesis and apoptosis. Biol Res. 2019;52:12.
48. Piret JP, Lecocq C, Toffoli S, Ninane N, Raes M, Michiels C. Hypoxia and CoCl2 protect HepG2 cells against serum deprivation- and t-BHP-induced apoptosis: a possible anti-apoptotic role for HIF-1, exp. Cell Res. 2004;295:340–9.
49. Dolomanov OV, Bourhis LJ, Gildea RJ, Howard JAK, Puschmann H. OLEX2: a complete structure solution, re-finement and analysis program. J Appl Crystallogr. 2009;42:339–41.
50. Sheldrick GM. SHELXS 97, program for the solution of crystal structure. Göttingen: University of Göttingen; 1990.

Publisher's Note